Pencil–paper on-skin electronics

Yadong Xu[a,1], Ganggang Zhao[b,1], Liang Zhu[c], Qihui Fei[a], Zhe Zhang[a], Zanyu Chen[b], Fufei An[d], Yangyang Chen[b], Yun Ling[b], Peijun Guo[e], Shinghua Ding[a,f], Guoliang Huang[b], Pai-Yen Chen[c], Qing Cao[d], and Zheng Yan[a,b,2]

[a]Department of Biomedical, Biological & Chemical Engineering, University of Missouri, Columbia, MO 65211; [b]Department of Mechanical & Aerospace Engineering, University of Missouri, Columbia, MO 65211; [c]Department of Electrical and Computer Engineering, University of Illinois at Chicago, Chicago, IL 60607; [d]Department of Materials Science and Engineering, University of Illinois at Urbana–Champaign, Urbana, IL 61801; [e]Department of Chemical & Environmental Engineering, Yale University, West Haven, CT 06516; and [f]Dalton Cardiovascular Research Center, University of Missouri, Columbia, MO 65211

Edited by James M. Tour, Rice University, Houston, TX, and accepted by Editorial Board Member John A. Rogers June 4, 2020 (received for review May 5, 2020)

Pencils and papers are ubiquitous in our society and have been widely used for writing and drawing, because they are easy to use, low-cost, widely accessible, and disposable. However, their applications in emerging skin-interfaced health monitoring and interventions are still not well explored. Herein, we report a variety of pencil–paper-based on-skin electronic devices, including biophysical (temperature, biopotential) sensors, sweat biochemical (pH, uric acid, glucose) sensors, thermal stimulators, and humidity energy harvesters. Among these devices, pencil-drawn graphite patterns (or combined with other compounds) serve as conductive traces and sensing electrodes, and office-copy papers work as flexible supporting substrates. The enabled devices can perform real-time, continuous, and high-fidelity monitoring of a range of vital biophysical and biochemical signals from human bodies, including skin temperatures, electrocardiograms, electromyograms, alpha, beta, and theta rhythms, instantaneous heart rates, respiratory rates, and sweat pH, uric acid, and glucose, as well as deliver programmed thermal stimulations. Notably, the qualities of recorded signals are comparable to those measured with conventional methods. Moreover, humidity energy harvesters are prepared by creating a gradient distribution of oxygen-containing groups on office-copy papers between pencil-drawn electrodes. One single-unit device (0.87 cm^2) can generate a sustained voltage of up to 480 mV for over 2 h from ambient humidity. Furthermore, a self-powered on-skin iontophoretic transdermal drug-delivery system is developed as an on-skin chemical intervention example. In addition, pencil–paper-based antennas, two-dimensional (2D) and three-dimensional (3D) circuits with light-emitting diodes (LEDs) and batteries, reconfigurable assembly and biodegradable electronics (based on water-soluble papers) are explored.

pencil–paper | biophysical | biochemical | energy harvester | on-skin electronics

On-skin electronics, also termed as epidermal electronics or skin-interfaced electronics, have demonstrated a variety of promising applications in human healthcare, human–machine interfaces, and virtual and augmented reality, among many others (1–10). Currently, on-skin electronics are usually made by patterning conventional inorganic electronic materials (e.g., copper, gold, silicon), novel organic electronic materials [e.g., poly(3,4-ethylenedioxythiophene) polystyrene sulfonate, poly(3-hexylthiophene)], or emerging nanomaterials (e.g., graphene, carbon nanotubes, silver nanowires) on mechanically compliant polymer supporting substrates (e.g., silicone elastomers, polyimide, polyethylene terephthalate) (1–10). Consequently, the state-of-the-art on-skin electronics often suffer from expensive precursor materials, costly fabrication facilities, complex fabrication processes, and limited disposability. For example, well-established fabrication procedures of on-skin electronics are usually associated with spin-coating, photolithography, vacuum deposition, and dry/wet etching, which are complicated, time-consuming, and expensive. Solution-based printing techniques can enable simple and scalable fabrication of flexible devices but usually suffer from expensive facilities, tedious efforts in ink formulations, and complex postprinting processes (11, 12). In addition, most polymer substrates used in on-skin electronics need hundreds of years to decompose in natural environments. Considering that on-skin electronics should be one-time use to minimize infection risks, their future wide implementation in our daily life would result in dramatic accumulations of electronic wastes. It is worth noting that emerging physically transient and recyclable bioelectronics might address the concerns of environmental pollutions (13, 14). However, their potentials are dampened by expensive precursor materials, costly fabrication facilities, and sophisticated fabrication processes.

Papers have a history of more than 2,000 y and have been widely used in our daily life ranging from packaging to printing and information display. Papers are usually made of natural cellulose fibers and can completely decompose within 6 wk. Also, papers are one of the most inexpensive materials (0.1 cent dm^{-2}) as compared to polymer substrates such as polyethylene terephthalate (≈2 cent dm^{-2}) and polyimide (≈30 cent dm^{-2}) (15). In addition, their high flexibility and breathability can benefit their applications in on-skin electronics. Pencils were invented in the 16th century and have been used for writing and drawing. Pencil lead is composed of fine graphite powers with various additives, by which pencils are classified into "H" and "B" categories. H and

Significance

On-skin electronics are usually fabricated by patterning conventional inorganic materials, novel organic materials, or emerging nanomaterials on flexible polymer substrates. Consequently, the state-of-the-art on-skin electronics usually suffer from expensive precursor materials, costly fabrication facilities, complex fabrication processes, and limited disposability. By using widely accessible pencils and papers as tools, we have developed a variety of cost-effective and disposable on-skin electronic devices, ranging from biophysical sensors and sweat biochemical sensors to thermal stimulators, humidity energy harvesters, and transdermal drug-delivery systems. Also, pencil–paper-based antennas, two-dimensional and three-dimensional circuits, and reconfigurable structures are demonstrated. The enabled devices can find wide applications particularly in low-resource environments and home-centered personal healthcare owing to their low-cost resources, handy operation, time-saving fabrication, and abundant potential designs.

Author contributions: Y.X., G.Z., and Z.Y. designed research; Y.X., G.Z., L.Z., Q.F., Z.Z., Z.C., F.A., Y.C., Y.L., P.G., S.D., G.H., P.-Y.C., and Q.C. performed research; Y.X., G.Z., and L.Z. analyzed data; and Y.X., G.Z., and Z.Y. wrote the paper.

The authors declare no competing interest.

This article is a PNAS Direct Submission. J.M.T. is a guest editor invited by the Editorial Board.

[1]Y.X. and G.Z. contributed equally to this work.

[2]To whom correspondence may be addressed. Email: yanzheng@missouri.edu.

This article contains supporting information online at https://www.pnas.org/lookup/suppl/doi:10.1073/pnas.2008422117/-/DCSupplemental.

B refer to hardness and blackness, respectively. The graphite particles are rubbed off due to friction between the pencil lead and the rough and porous paper substrate in a writing cycle, where conductive graphite flakes are transferred to papers. Despite the recent progress of their applications in supercapacitors and strain gauges (16, 17), pencil–paper-based on-skin electronic devices, which can stick to human bodies for a long term, record vital biophysical and biochemical signals in a high-fidelity fashion, harvest energy from ambient humidity, and deliver programmed physical and chemical interventions, are still lacking.

In this work, we explore the pencil drawing of a variety of bioelectronic devices on commonly used office-copy papers with commercial 9B pencils. Here, pencil-drawn graphite patterns (or combined with other compounds) work as conductive traces and sensing electrodes, and papers serve as flexible supporting substrates as well as the basis materials for ambient humidity energy harvesters. Besides, a trace amount of adhesive materials (Silbione RT Gel 4717 A/B; Elkem Silicones; the weight ratio of Silbione and paper: ~5:100) is spray-coated onto the bared regions of pencil–paper on-skin electronics to improve the skin–device adhesion. The

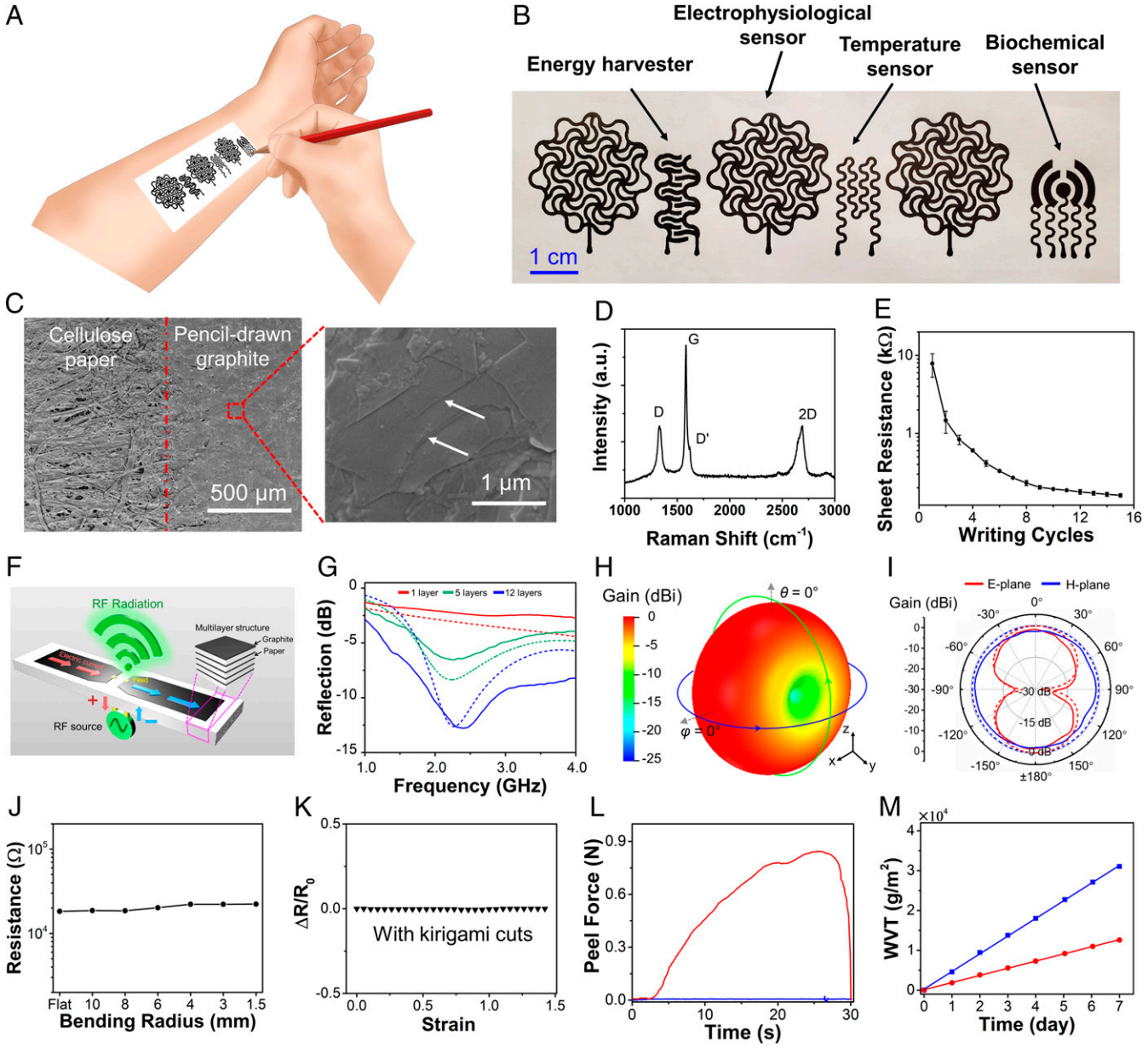

Fig. 1. Pencil drawing of on-skin electronics on papers. (*A*) Conceptual illustrations of drawing on-skin electronics on papers using a 9B sketching pencil. (*B*) A photograph of pencil–paper on-skin electronics. (*C*) SEM images of pencil-drawn graphite on papers. Arrows indicate the multilayer structures and edges of graphitic flakes. (*D*) Raman spectrum of pencil-drawn graphite on papers. (*E*) Variations in the sheet resistance of pencil-drawn graphite on papers as a function of writing cycles. Error bars represent the SDs of three individual samples. (*F*) Schematic of a planar dipole antenna based on the multilayered structure of pencil-drawn graphite and paper. (*G*) Reflection (S_{11}) spectra for the pencil–paper-based dipole antenna with different numbers of stacked layers (5G midband). (*H* and *I*) Simulated 3D (*H*) and simulated and measured 2D (*I*) radiation patterns for the pencil–paper-based dipole antenna (12 layers) working at 2.3 GHz. In *G* and *I* solid and dashed lines represent the measurement and simulation results, respectively. (*J* and *K*) Variations in the electrical resistance of pencil-drawn graphite as a function of bending radius (*J*) and tensile strain (*K*). (*L*) Peel–adhesion tests of pristine papers (blue) and papers with spray-coated Silbione (red) on the forearm of a human volunteer, indicating the significantly enhanced adhesion after Silbione coating. The sample size is 1.5 × 4 cm^2. (*M*) Water vapor transmissions (WVT) of pristine papers (blue) and papers coated with Silbione (red) as a function of the elapsed time.

prototypic device examples include temperature sensors, electrophysiological (i.e., biopotential) sensors, electrochemical sweat sensors, joule-heating elements, and ambient humidity energy harvesters, that can 1) record a variety of vital biophysical information from bodies [including skin temperatures, electrocardiograms (ECGs), electromyograms (EMGs), alpha, beta, and theta rhythms, instaneous heart rates, and respiratory rates] in a real-time, continuous, and high-fidelity manner, as well as provide programmed thermal stimulations; 2) *in situ* analyze three proof-of-concept sweat biomarkers, including pH, uric acid (UA), and glucose, with high sensitivity and selectivity; and 3) generate a sustained voltage of up to 480 mV per single unit (0.87 cm^2) for over 2 h. In addition, a self-powered transdermal drug-delivery system is developed as an example of on-skin chemical interventions. Besides, pencil–paper-based antennas, 2D/3D circuits with LEDs and batteries, biodegradable electronics (based on water-soluble paper) and reconfigurable assembly are explored. The fabrication and characterization are detailed in *SI Appendix, Methods*.

Results

Pencil Drawing of On-Skin Electronics on Papers. Pencil lead is usually composed of graphite, clay, and wax. High graphite contents could enable drawing of high-electrical-conductivity patterns on papers. Here, a 9B sketching pencil with ∼93% graphite content by weight is used for drawing of a variety of on-skin bioelectronic devices on office-copy papers (∼100 μm thick; Staples Inc; Fig. 1*A*). Fig. 1*B* provides a typical optical image of fabricated on-skin bioelectronic devices, including temperature sensors, electrophysiological sensors, sweat electrochemical sensors, and humidity energy harvesters, which have open-mesh, serpentinelike layouts. Similar device layouts of temperature sensors can also be used as joule-heating elements. Scanning electron microscope (SEM) images show that graphitic materials are successfully transferred from the pencil lead to the rough and porous cellulose paper substrate, where a boundary is clearly observed (Fig. 1*C* and *SI Appendix*, Fig. S1 *A* and *B*). The shear-peeling force of the direct-drawing process creates multilayer graphitic materials with a large amount of open-edge structures due to their anisotropic mechanical properties. Raman spectrum of pencil-drawn graphite on papers shows characteristic spectrum with three main peaks centered at 1,332, 1,582, and 2,691 cm^{-1}, which can be attributed to D, G, and 2D bands, respectively (Fig. 1*D*) (18). The G band is due to the in-plane E_{2g} mode, which arises from the stretching of C–C bond, while D and D′ bands can be attributed to the defects at the graphite edges. The electrical conductivity of pencil-drawn graphitic materials on papers is systematically investigated by orthogonally ruler-guided drawing for a number of cycles. As shown in Fig. 1*E*, the sheet resistance of pencil-drawn graphite is inversely correlated with writing cycles, increasing from ∼10 kΩ sq^{-1} at the first cycle to ∼160 Ω sq^{-1} at the 15th cycle. In this research, 15 writing cycles were used for the fabrication of on-skin devices with the thickness of graphite layers at ∼6 μm (*SI Appendix*, Fig. S1*C*). Also, the patterns drawn by 9B pencils exhibit better electrical conductivities than the ones drawn by others largely because of their higher graphite contents (*SI Appendix*, Fig. S2).

The high electrical conductivity of pencil-drawn traces on office-copy papers makes them well suitable for a variety of on-skin electronic devices (e.g., biophysical and biochemical sensors, humidity energy harvesters, antennas, interconnects). To exemplify their potential use in radio-frequency (RF) and wireless communication applications, we have applied the pencil-drawing method to build a low-profile planar dipole antenna onto the office-copy paper substrate (Fig. 1 *F–I* and *SI Appendix*, Fig. S3). Center-fed half-wavelength dipole antennas with an omnidirectional radiation pattern are widely used for radio transmitting and receiving applications (19). Fig. 1*F* shows the schematic of this type of antenna with its dipole arms formed by multiple layers of pencil-drawn graphite on paper. The in-phase oscillating alternating currents induced on dipole arms generate an omnidirectional radiation pattern in the far-field (Fraunhofer) region. Intuitively, increasing the number of stacked pencil–paper layers can reduce the sheet resistance, thus enhancing the radiation efficiency and the realized gain of RF antennas (*SI Appendix*, Fig. S3). Fig. 1*G* presents the reflection coefficient (S_{11}) for half-wavelength dipole antennas consisting of 1, 5, and 12 layers (see *SI Appendix*, Fig. S3*C* for the manufactured antenna on the paper substrate). We find that measurement results agree well with simulated ones, indicating that increasing the number of layers of pencil-drawn graphite on paper can improve the impedance matching condition, owing to the reduction of the antenna's loss resistance (which is associated with the effective sheet resistance). When 12 layers of pencil-drawn graphite on paper are used, a −10-dB bandwidth of 0.77 GHz can be achieved at 2.3 GHz (4G LTE and Bluetooth band). Fig. 1 *H* and *I* present the simulated and measured radiation patterns at 2.3 GHz for the 12-layer pencil–paper-based antenna. We find a good agreement between numerical simulations and experimental results, showing that the maximum realized gain is ∼ −1.63 dBi. This value is slightly lower than that of an ideal half-wavelength dipole made of perfect conductor (2.15 dBi), but is comparable to those measured from the-state-of-the-art flexible dipoles made of conductive polymers (20), inkjet-printed metals (21), and thin-film metal (22). Finally, we should note that the realized gain can be further improved by stacking more pencil–paper layers. According to our simulation results, a realized gain of 0.80 dBi can be achieved by stacking 25 pencil–paper layers. This simple and low-cost manufacturing technique may open up avenues for development of flexible and disposable RF electronics (e.g., radio-frequency identification (RFID) and Internet of Things (IoT) tags). In addition, as shown in *SI Appendix*, Fig. S4 and Movie S1, pencil-drawn interconnects on office-copy papers can integrate with commercial electronic components (e.g., LEDs, batteries) in both 2D and 3D circuits. These results, together with the results of bioelectronic sensors and humidity energy harvesters that are described subsequently, indicate the possibility of developing pencil–paper-based whole wearable systems, which is worth exploring in the future.

Besides, the open-mesh, serpentinelike layout was adopted for the fabrication of bioelectronic devices in Fig. 1*B* mainly because electrical performances of such structures are less susceptible to mechanical deformations. For example, only a small resistance change (∼20%) was observed at a bending radius of 1.5 mm (Fig. 1*J*). In addition, we adopt kirigami cuts (23) to overcome the papers' intrinsically poor stretchability (*SI Appendix*, Fig. S5). With kirigami cuts, the electrical resistance of pencil-drawn, serpentinelike graphite patterns show no measurable change under up to ∼150% tensile strain (Fig. 1*K*). Moreover, after 1,000 cycles of bending tests (bending radius: 6 mm) and uniaxial stretching tests (tensile strain: 100%), only ∼8 and ∼0.1% resistance changes were observed, respectively (*SI Appendix*, Fig. S6). Such excellent electromechanical performances are sufficient for a broad range of on-skin bioelectronic applications considering relatively small natural deformations of human skins (bending: >∼140 mm for chest and >∼50 mm for foot; stretching: up to 50–80%) (10, 24). Furthermore, commonly used office-copy papers are not sticky and cannot form intimate contact with the skin, which is of extreme importance for long-term and high-fidelity recording of vital physiological signals from human bodies. To overcome this handicap, we spray-coat Silbione, which is biocompatible and has low elastic modulus (∼3.0 kPa), onto bare regions of on-skin electronic devices to improve their stickiness. As shown in Fig. 1*L*, a trace amount of Silbione coating can dramatically improve the stickiness of the resulting on-skin electronic devices. The measured adhesion force from the forearm of a human volunteer increases from

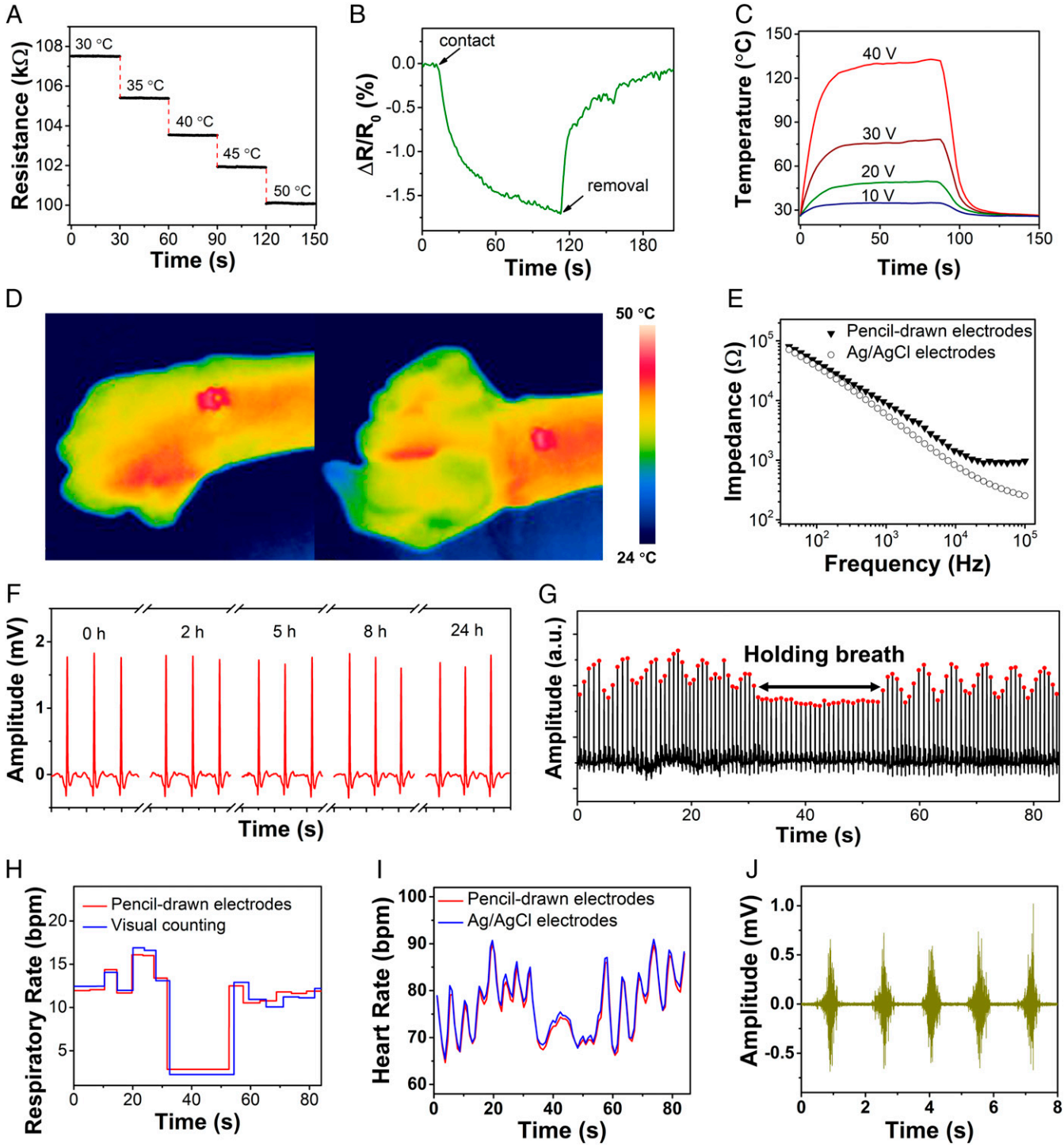

Fig. 2. On-body evaluations of pencil–paper on-skin biophysical sensors and thermal stimulators. (*A* and *B*) Dynamic electrical responses of the pencil–paper on-skin temperature sensor on a hotplate with various fixed temperatures (*A*) and upon contact and removal from the human skin (*B*). (*C*) Temperature–time profiles of the pencil–paper on-skin joule-heating element with applied voltages of 10, 20, 30, and 40 V. (*D*) Infrared thermal camera images of the pencil–paper on-skin joule-heating element laminated on the wrist of a human volunteer with an applied voltage of 15 V. (*E*) Impedances of the skin–electrode interface of pencil-drawn graphite electrodes and conventional Ag/AgCl electrodes, measured from the forearm of a human volunteer. (*F*) Long-term ECG recording from the chest of a human volunteer using the pencil–paper on-skin electrophysiological sensor, indicating high stability. (*G*) Dynamic amplitude responses of the R peaks in the ECG signals while the volunteer held the breath for ∼25 s. (*H*) Respiratory rates determined by the R peak amplitude variations in *G* and visual counting by a physician. (*I*) Comparisons of instantaneous heart rates determined from the R-to-R peak intervals in the ECG signals recorded with pencil–paper on-skin sensors and conventional Ag/AgCl electrodes. (*J*) EMG signals recorded from the forearm of a human volunteer with the pencil–paper on-skin sensor.

∼0.01 to ∼0.85 N after Silbione coating. Here, the weight ratio of the spray-coated Silbione and paper is ∼5:100. The enabled sticky pencil–paper on-skin devices can stay on human bodies for more than 3 d. Besides, high breathability is desirable for on-skin electronics, which can expedite skin perspiration evaporation, minimize sweat accumulation, and alleviate inflammatory reactions

(25–27). As shown in Fig. 1*M*, after Silbione coating, the paper still exhibits a decent water vapor transmission rate (2,137 g m^{-2}·day^{-1}), which is sufficiently higher than that of human skin (204 g m^{-2}·day^{-1}) (28). The optimal amount of spray-coated Silbione is obtained based on a trade-off between the stickiness and breathability (*SI Appendix*, Fig. S7). Here, Silbione is used to improve the skin adhesion of commonly used office-copy papers. Notably, our results also demonstrate that pencils can be used to directly draw high-quality bioelectronic devices on commercially available adhesive papers without needing additional Silbione coating to further simplify the fabrication process. More details are provided in subsequent sections.

On-Body Evaluations of Pencil–Paper On-Skin Biophysical Sensors and Thermal Stimulators. The continuous and high-fidelity monitoring of skin temperatures and electrophysiological signals can facilitate an understanding of an individual's evolving physiological state and stress levels (1, 29). The pencil–paper on-skin temperature sensor consists of a pencil-drawn graphite conductive trace, with a negative temperature coefficient (−0.36% $°C^{-1}$), calibrated using a thermocouple (*SI Appendix*, Fig. S8). The enabled devices demonstrate fast electrical responses to temperature changes and can work well in the physiological temperature range (Fig. 2*A*). The electrical resistance of the temperature sensor decreased by ∼1% immediately upon contact with the forearm of a human volunteer and fully reverted to its initial value upon removal from the volunteer forearm (Fig. 2*B*). The similar device layout can also be used as the on-skin joule-heating element, which are useful for biomedical treatment (e.g., wound healing). Fig. 2*C* provides the temperature–time profiles of pencil–paper on-skin joule-heating elements with various applied voltages. The temperature exhibits sharp increase from room temperature to ∼125 °C within 30 s when 40-V voltage is applied owing to the graphite's high thermal conductivity. Fig. 2*D* demonstrates that the enabled devices can maintain stable thermal stimulations even when the human wrist is flexed and extended. Furthermore, *SI Appendix*, Fig. S9 demonstrates that pencil-drawn joule heaters on papers can serve the basis to enable electrothermally triggered reversible assembly, which can open up research and application avenues of pencil-on-paper methods in reconfigurable and responsive devices, 3D functional devices, and soft robotics (30).

The on-skin electrophysiological sensor consists of pencil-drawn reference, ground, and measurement electrodes. Fig. 2*E* shows that the skin–device contact impedance of pencil-drawn electrophysiological electrodes is ∼40 kΩ at 100 Hz, comparable to conventional silver/silver chloride (Ag/AgCl) gel electrodes (∼37 kΩ at 100 Hz). The magnified ECG signal indicates distinguishable P-wave, QRS complex, and T-wave (*SI Appendix*, Fig. S10*A*). As shown in *SI Appendix*, Fig. S10*B*, the signal-to-noise ratio (SNR) of the ECG signals, recorded with pencil–paper on-skin electrophysiological sensors, is ∼30 dB, comparable to the results measured from Ag/AgCl electrodes (∼32 dB). Fig. 2*F* and *SI Appendix*, Fig. S11 show that pencil–paper on-skin electrophysiological sensors can measure ECG from human chests in a continuous and high-fidelity manner. The SNR ratios of the recorded ECG signals before and after continuous measurement for 24 h are 30.9 and 32.6 dB, respectively, indicating high stability. *SI Appendix*, Fig. S12 demonstrates the ECG signals recorded by 20 randomly selected devices from the chest of a volunteer (with the mean value of the SNR at 33.2 dB and the SD at 3.4 dB), displaying high reproducibility. Furthermore, respiratory rates can be determined from the recorded ECG signals by analyzing intrathoracic impedance variations caused by human breathing (31). Specifically, the R peak amplitude in QRS complex decreases as the intrathoracic impedance increases during the inspiration, while it increases as the latter decreases during the expiration, and no obvious amplitude change is observed when holding breath (Fig. 2*G* and *SI Appendix*, Fig. S13). The extracted respiratory rates match well with those obtained by visual counting (Fig. 2*H*). Meanwhile, instantaneous heart rates (containing the information of heart rates and heart-rate variations) can be determined by the R-to-R intervals of the ECG signals recorded with pencil–paper on-skin electrophysiological sensors, which agree well with the results extracted from the ECG signals measured with Ag/AgCl electrodes (Fig. 2*I*). In addition, Fig. 2*J* and *SI Appendix*, Fig. S14 demonstrate that EMG signals with an SNR of ∼30 dB can be collected from the forearm (flexor carpi radialis muscle) of a human volunteer using pencil–paper on-skin electrophysiological sensors, which are quantitatively comparable to the data recorded with Ag/AgCl electrodes (∼32 dB). The real-time EMG recording is useful in human–machine interfaces (25). Notably, the on-skin electrophysiological sensors based on commonly used office-copy papers remain stable and reliable under heavy skin perspirations (*SI Appendix*, Fig. S15) and even after direct water infusion (*SI Appendix*, Fig. S16).

In addition, high-quality electrophysiological sensors can be directly drawn with pencils on commercial adhesive papers (Aquasol water-soluble paper for this demonstration) without needing Silbione coating to further simplify fabrication processes (*SI Appendix*, Fig. S17). Interestingly, pencil-drawn bioelectronic devices on water-soluble papers are biodegradable and can dissolve in water rapidly (Movie S2). Also, the obtained devices can be transferred onto curvy human bodies after dissolving water-soluble paper substrates. The substrate-free pencil-drawn devices can still record high-fidelity electrophysiological signals from human bodies (*SI Appendix*, Fig. S18).

Monitoring of Cerebral Activities via Real-Time Electroencephalogram Recording. Continuous monitoring of cerebral activities via high-fidelity, real-time electroencephalogram (EEG) recording is of critical importance for studying cognitive behaviors and can also provide insights into various neurological disorders and human fatigue (32–34). Cerebral activities can be divided into five frequency bands: delta wave (0–4 Hz), theta wave (4–8 Hz), alpha wave (8–12 Hz), beta wave (12–40 Hz), and gamma wave (>40 Hz) (35). Each frequency band is associated with different mental states. For example, high-frequency, low-amplitude beta waves are often observed during intensive, complex, attentional mental states (36). Pencil–paper on-skin electrophysiological sensors can be used to monitor cerebral activities via real-time EEG recording when human subjects engage in different mental states (Fig. 3*A*). During the testing, the subject was asked to first close eyes, then open eyes and maintain a twilight state (i.e., dreamy state without awareness of the surroundings), and finally do complex math calculations. Each mental state was maintained for 90 s and there was a 5-min break between each state. The recorded EEG signals reveal intense high-frequency cerebral activities during math calculation and strong low-frequency cerebral activities during closed eyes and twilight state (Fig. 3*B*). Fast Fourier transform (FFT) was further applied to analyze the recorded EEG signals (Fig. 3*C*), indicating clear alpha wave (∼10 Hz) for closed eyes, theta wave (∼6.5 Hz) for twilight state, and beta wave (∼28 Hz) for math calculation. The time–frequency spectrograms of recorded EEG signals show clear differences in signal intensities during three mental states (Fig. 3*D* and *SI Appendix*, Fig. S19).

Characterization and On-Body Evaluation of Pencil–Paper-Based On-Skin Biochemical Sensors. In situ perspiration biochemical analysis, together with real-time measurement of biophysical signals, can provide a dynamic and complete picture of human health states (3, 6, 37). As proof-of-concept examples, we have developed pencil–paper-based sweat pH, UA, and glucose sensors (Fig. 4 and *SI Appendix*, Figs. S20–S25). Fig. 4*A* and *SI Appendix*, Fig. S20 provide the schematic illustrations and working mechanisms of pencil–paper-based on-skin biochemical sweat sensors. pH sensors

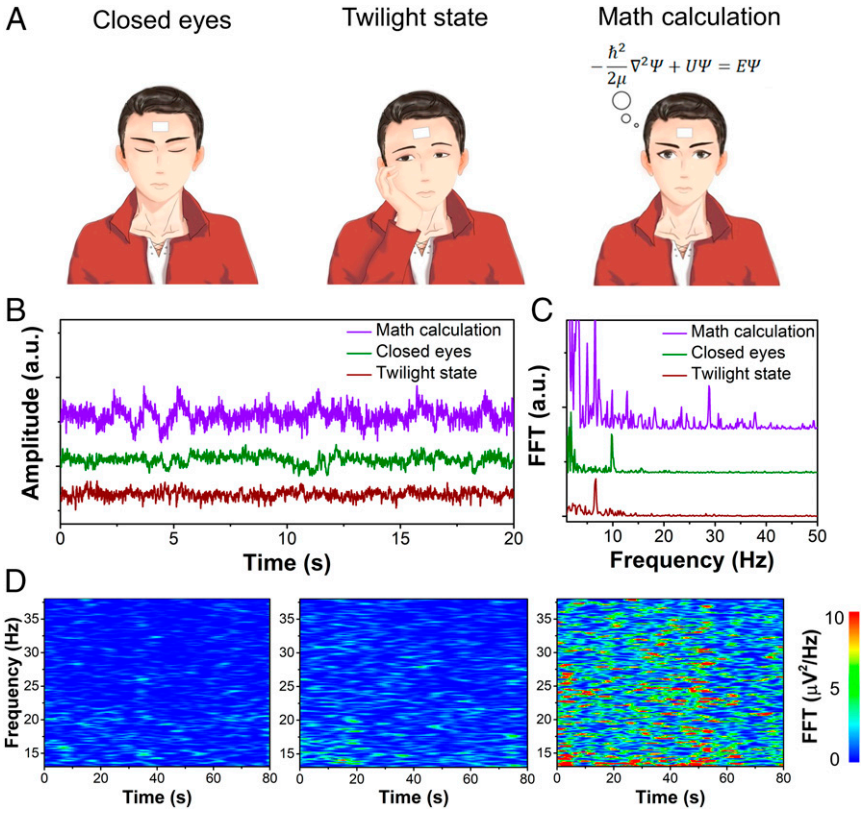

Fig. 3. Monitoring of cerebral activities via real-time EEG recording. (*A* and *B*) Schematics (*A*) and recorded EEG signals (*B*) using pencil–paper on-skin electrophysiological sensors when a human volunteer engaged in three mental states. (*C*) FFT-processed frequency distributions of the EEG signals in *B*. (*D*) Time–frequency spectrograms of the EEG signals within beta band (13–38 Hz) during three mental states (*Left*: closed eyes; *Middle*: twilight state; *Right*: math calculation), showing significantly higher signal intensities during math calculation.

consist of polyaniline (PANi)-coated pencil-drawn graphite working electrodes and Ag/AgCl ink-coated pencil-drawn graphite reference electrodes, which are used to record the dynamic responses of open-circuit potentials (OCPs) at different pH levels. The pH sensors are calibrated in standard buffer solutions and exhibit stable signals from pH 3 to 10 (Fig. 4*B*). The enabled pH sensors are reliable over continuous use at different pH levels and have an average sensitivity of 35 mV/decade (Fig. 4*C*). The UA sensors consist of working, reference, and counter electrodes, which can be used to measure UA concentrations with the differential pulse voltammetry (DPV) method. The current peaks of the UA sensors in DPV signals are attributed to the selective oxidation of UA at ∼0.3 V (Fig. 4*D*). The pencil–paper-based UA sensor exhibits a good linear relationship with a high sensitivity of ∼21.9 nA μM^{-1} in the range of 0–600 μM (Fig. 4*E*) and high selectivity over other interferential sweat analytes (Fig. 4*F*), including glucose (Glu), lactate (LA), and ascorbic acid (AA). The amperometric glucose sensor consists of pencil-drawn graphite working electrodes functionalized with gold nanoparticles (AuNPs), Prussian blue and glucose oxidase (GOx), and Ag/AgCl ink-coated pencil-drawn graphite reference electrodes. The glucose sensors indicate a dynamic current response over the glucose concentration range of 0–90 and 90–600 μM, showing linear relationships between current and glucose concentration with the sensitivities of 1.64 and 3.04 nA μM^{-1}, respectively (Fig. 4 *G* and *H* and *SI Appendix*, Fig. S21). The enabled glucose sensor exhibits negligible signal variations with the addition of a variety of interferential biomarkers (AA, LA, UA), demonstrating a good selectivity (Fig. 4*I*). The pencil–paper-based sweat sensors are reproducible and stable (*SI Appendix*, Figs. S22 and S23). Besides, the effects of physiological pH and temperature variations on glucose and UA sensors were investigated and are provided in *SI Appendix*, Figs. S24 and S25. Notably, pencil–paper-based biochemical sweat sensors demonstrate comparable performances with the ones made of advanced carbon materials (38, 39) in terms of sensitivity and selectivity.

To further demonstrate the capability of pencil–paper-based sweat sensors, we laminated the devices onto the forehead of one volunteer for real-time perspiration analysis. Also, the raw sweat samples were collected and analyzed using conventional methods. Here, glucose, pH, and UA were analyzed with high-performance liquid chromatography (HPLC), a commercial pH meter, and commercial colorimetric assay kits (38), respectively. As shown in Fig. 4*J*, the data measured with pencil–paper-based sweat sensors from human bodies after heavy perspirations match well with the results obtained using these conventional approaches. Continuous on-body monitoring of UA concentrations before and after a purine-rich diet (300 g of canned sardines for this study) over a 9-h period is provided in Fig. 4*K*, further demonstrating the capability of pencil–paper-based sweat biochemical sensors for continuous, in situ perspiration analysis.

Characterization of Pencil–Paper-Based Ambient Humidity Energy Harvesters and Development of a Self-Powered On-Skin Transdermal Drug-Delivery System. It is highly desirable to develop ambient on-skin energy harvesters to enable self-powered wearable biomedical systems. Pencil–paper-based energy harvesters, which can generate electricity from ambient humidity, are explored in this research. Here, a moisture–electric polarization process (40) was used to create a gradient of oxygen-containing groups (e.g., hydroxyl groups, carboxyl groups) on constituent cellulose fibers of office-copy papers between pencil-drawn interdigital graphite electrodes (Fig. 5*A* and *SI Appendix*, Figs. S26 and S27). The

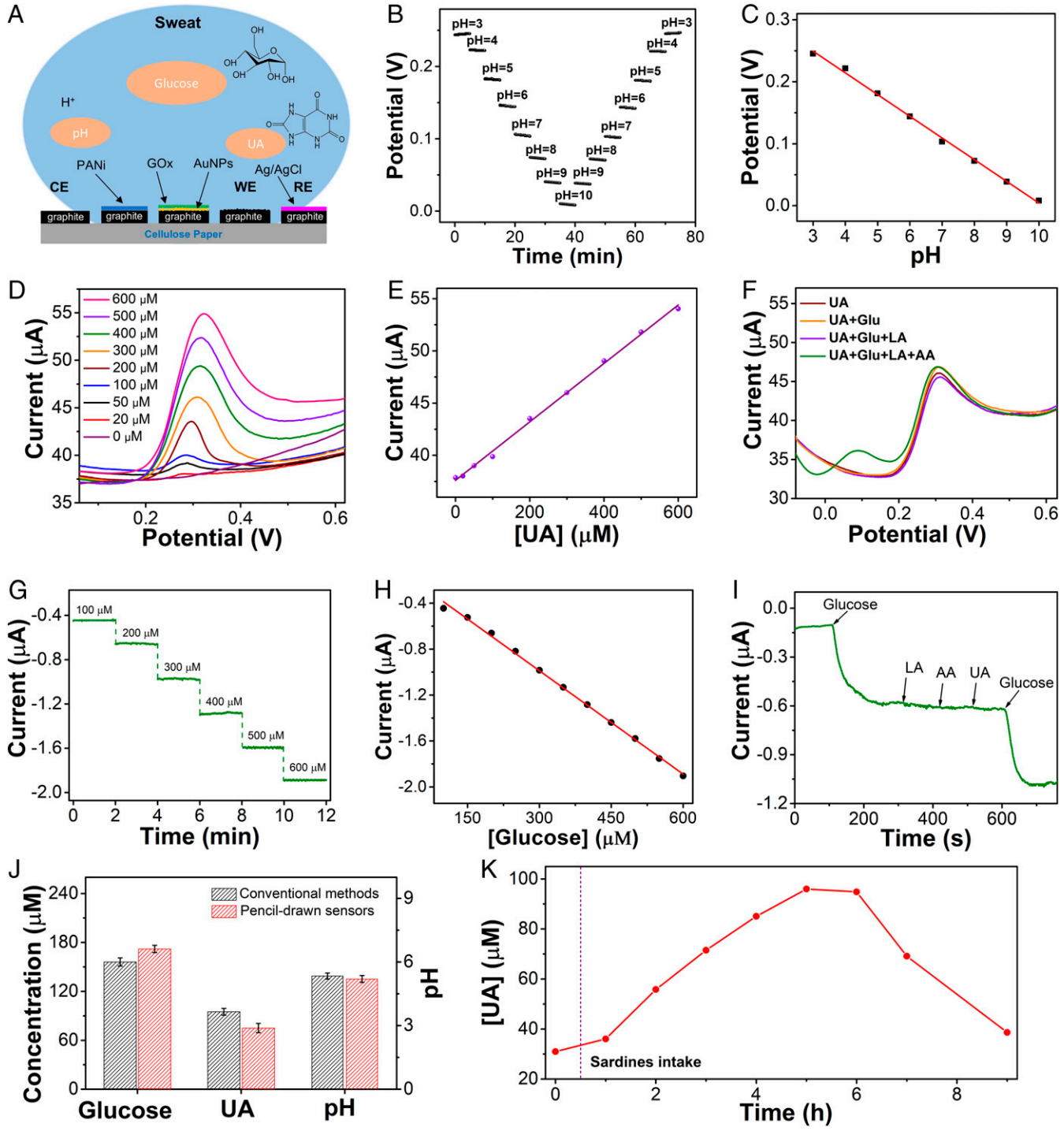

Fig. 4. Characterizations and perspiration analysis of pencil–paper-based pH, UA, and glucose sensors. (*A*) Schematic illustrations of pencil–paper-based sweat biochemical sensors for *in situ* measurement of pH, UA, and glucose in sweat. CE: counter electrode; WE: working electrode; RE: reference electrode. (*B*) Dynamic OCP responses to pH variations. (*C*) Calibration plot of the pH sensor. (*D* and *E*) DPV responses (*D*) and calibration plot (*E*) of the UA sensor over the concentration range of 0–600 μM in a 0.1 M phosphate buffer solution (pH 7.2). (*F*) Selectivity test of the UA sensor. (*G* and *H*) Dynamic current responses to glucose concentration variations (*G*) and calibration plot (*H*) of the glucose sensor. (*I*) Selectivity test of the glucose sensor. (*J*) Comparisons of the data measured with pencil–paper-based biochemical sensors and the results obtained with the conventional methods. (*K*) Dynamic change of the UA concentrations, recorded by pencil–paper-based UA sensors, before and after a purine-rich diet over a 9-h period.

oxygen-containing groups can absorb water molecules from the environment and generate a concentration gradient of hydrogen ions via a hydrolysis effect. Subsequently, the diffusion of hydrogen ions driven by the concentration gradient can generate electricity. Both X-ray photoelectron spectroscopy (XPS) analysis and line-scan energy-dispersive X-ray spectroscopy (EDS) demonstrate the existence of a gradient distribution of oxygen-containing groups on polarized office-copy papers (Fig. 5 *B* and *C* and *SI Appendix*, Fig. S28). In particular, XPS spectrum indicates that from the cathode to the anode, the C-C peak is clearly weakened whereas the C-O

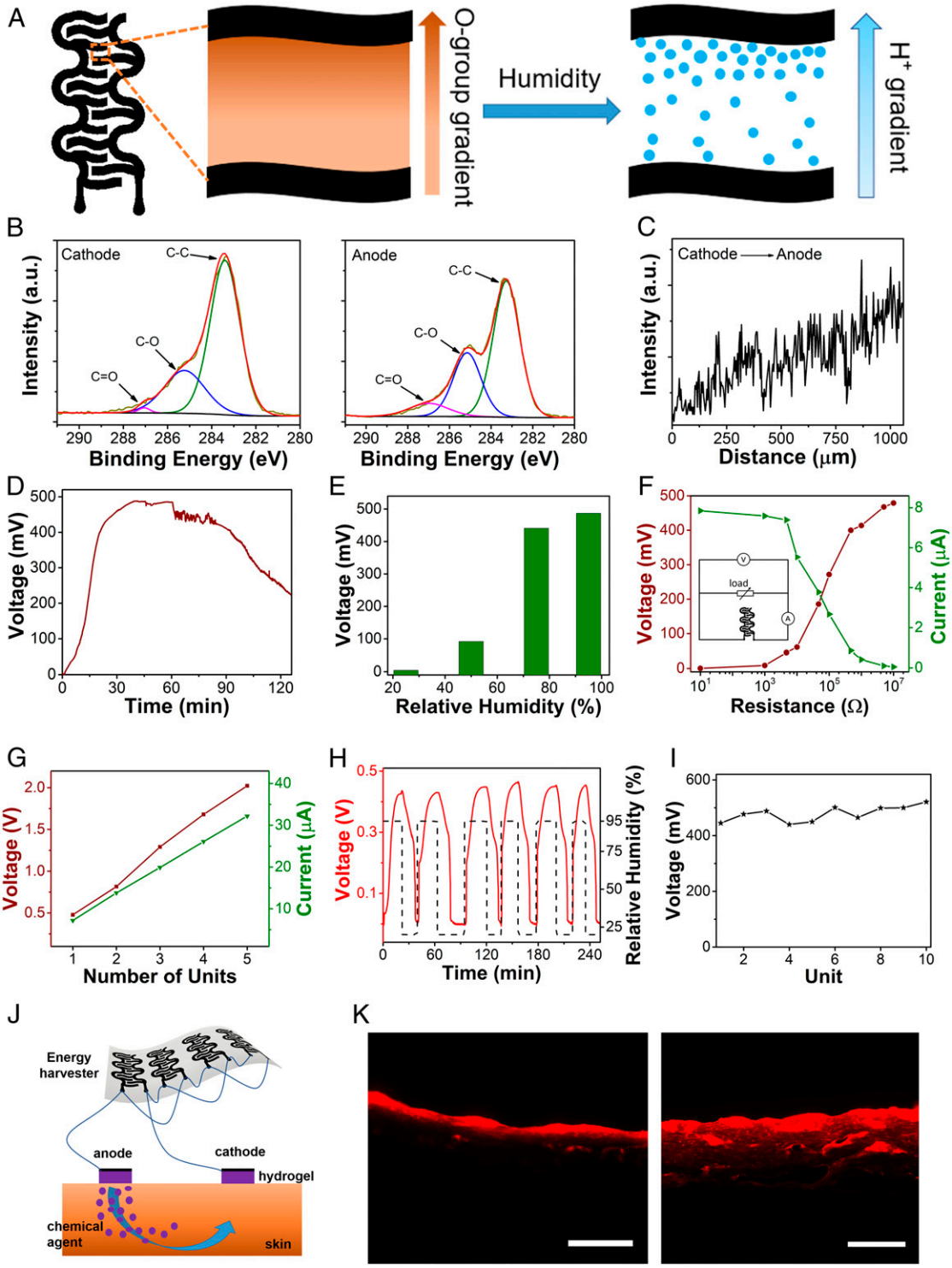

Fig. 5. Characterization of pencil–paper-based humidity energy harvesters and demonstration of self-powered on-skin transdermal drug-delivery systems. (*A*) Schematic illustrations of humidity energy harvesters, enabled by creating a gradient of oxygen-containing groups on cellulose papers between interdigital pencil-drawn graphite electrodes via a moisture–electric polarization process. (*B*) High-resolution C 1s XPS spectra of the polarized cellulose paper near the cathode (*Left*) and the anode (*Right*), which can be deconvoluted into three subpeaks, representing C–C, C = O, and C–O bonds, respectively. (*C*) Line-scan EDS of the polarized cellulose paper between two pencil-drawn graphite electrodes, showing an increased oxygen atomic ratio from the cathode to the anode. (*D*) Dynamic responses of the open-circuit voltage of energy harvesters exposed to a relative humidity of ~95% as a function of the elapsed time. (*E*) Correlations of the output voltage and environmental humidity. (*F*) Output voltages and output currents of energy harvesters connected with external resistors with different resistances. (*Inset*) Circuit layout used for testing. (*G*) Electrical performances of energy-harvester units connected in series (red) and in parallel (green). (*H*) Dynamic responses of the output voltage to intermittent and periodic humidity variations, showing high cyclic stability and self-charging capability. (*I*) Output voltages of 10 randomly selected devices with a mean of 478.6 mV and an SD of 27.7 mV, demonstrating high reproducibility. (*J*) Schematic of a self-powered on-skin transdermal drug-delivery system. (*K*) Cross-sectional fluorescent images of pig skins without (*Left*) and with (*Right*) iontophoresis. (Scale bars, 200 μm.)

and C = O peaks become stronger. And, EDS spectrum shows that the O/C atomic ratio increased from 0.75 (near the cathode) to 0.92 (near the anode).

The enabled energy harvester (effective device area: ~0.87 cm^2) can generate a sustained open-circuit voltage (V_o) of up to ~480 mV for more than 2 h when exposed to a relative humidity of ~95% (Fig. 5*D*), indicating comparable performances with recently developed, humidity energy harvesters that are made of advanced functional materials (e.g., graphene oxide, polyelectrolyte membrane) (40, 41). Fig. 5*E* indicates that the peak output voltage is positively correlated with the environment humidity, mainly because the higher humidity can lead to higher carrier quantities and low ionic resistances. Fig. 5*F* illustrates the responses of the output voltage and current of energy harvesters to external resistor loads with different resistances, indicating a peak output voltage of ~480 mV with a 10-MΩ external resistor and a peak output current of ~8 μA with a 10-Ω external resistor (*SI Appendix*, Fig. S29). Furthermore, the output voltage and current can be easily scaled up by connecting multiple energy-harvesting units in series or in parallel (Fig. 5*G*). For example, a five-unit device can provide a peak open-circuit voltage of ~2.1 V in series and peak short-circuit current of ~32 μA in parallel, demonstrating potentials for different biomedical applications. In addition, Fig. 5*H* indicates that paper–pencil-based humidity energy harvesters can be reused for multiple times since the generated voltage can be restored through self-recharging processes. Besides, the enabled energy harvesters are highly reproducible (Fig. 5*I* and *SI Appendix*, Fig. S30).To demonstrate the capability of pencil–paper-based on-skin humidity energy harvesters, we develop a proof-of-concept self-powered iontophoretic transdermal drug-delivery system (Fig. 5*J*). Here, poloxamer 407-based hydrogel is used as the drug carrier and cationic rhodamine B dye is used as the model drug. Transdermal drug delivery is demonstrated on pig skins. In the research, the device, assembled with eight energy-harvesting units in parallel, was used to provide the stimulation electricity for iontophoresis at a relative humidity of ~95%. As illustrated by the fluorescent images in Fig. 5*K*, the model drug was successfully transported from the hydrogel to the pig skin along the direction of the current flow via the iontophoresis process.

Conclusion

In summary, we report the fabrication and evaluation of a rich variety of pencil–paper-based skin-interfaced bioelectronic devices, ranging from biophysical sensors and sweat biochemical sensors to thermal stimulators, ambient humidity energy harvesters, and transdermal drug-delivery systems. The enabled devices can record a broad spectrum of vital physiological signals from human bodies in a high-fidelity and continuous manner, generate sustained electricity from ambient humidity, and deliver on-skin physical (thermal stimulations) and chemical (transdermal drug-delivery) interventions in a programmed manner. Also, pencil–paper-based antennas, 2D and 3D circuits with commercial LEDs and batteries, biodegradable devices, and reconfigurable assembly are explored. These comprehensive demonstrations in emerging on-skin wearables not only will grant this ancient and ordinary pair of tools (i.e., pencils and papers) vigor and vitality, but also can broaden the impacts of skin-interfaced human health monitoring and interventions in general. It is worth noting that pencil–paper-based methods cannot achieve as high patterning resolutions as other advanced fabrication techniques (such as photolithography and solution printing) but can work as valuable complements to the state-of-the-art fabrication methods of on-skin electronic devices. For example, pencil–paper-based on-skin devices can serve as propaganda and inspirational materials for education and training purposes, and also can find wide applications in low-resource environments and home-centered personalized healthcare owing to their low-cost resources, handy operation, time-saving fabrication, and abundant potential designs.

Methods

Details in materials, fabrications, and characterizations of pencil–paper-based devices are provided in *SI Appendix*. Briefly stated about the signal recording, electrophysiological signals were measured based on the three-electrode layout with PowerLab T26 (AD Instruments), where the potential difference between the recording electrode and reference electrode was measured. The ground electrode provided a zero-potential point for determining the potential difference between the recording electrode and reference electrode. Changes in the resistance of the temperature sensor were measured using an LCR meter (IM3523, HIOKI). Electrochemical characterizations were conducted on an electrochemical station (CHI660E, CH Instruments, Inc.). For pH sensing, the dynamic responses of OCP between the working electrode and Ag/AgCl reference electrode were recorded at different pH levels. The UA sensors were evaluated by the oxidation peak currents at 0.3 V (vs. Ag/AgCl reference electrode) using the DPV method. For glucose sensing, chronoamperometry was employed, which gives a current (I) versus time (t) curve under a constant potential of -0.05 V (vs. Ag/AgCl reference electrode), and various currents were obtained at different glucose concentrations. The output voltages and currents of humidity energy harvesters are of the opposite sign and were measured by a digital sourcemeter (2604B, Keithley Instruments Inc.). Their absolute values are used in this study.

Experiments on Human Subjects. The on-body evaluations of on-skin devices on five human volunteers were conducted under approval from Institutional Review Board at the University of Missouri-Columbia (Project number: 2010272). All human subjects gave written and informed consent before participation in the studies.

Data and Materials Availability. All data needed to evaluate the conclusions in the paper are present in the paper, *SI Appendix*, and Movies S1 and S2.

ACKNOWLEDGMENTS. Z.Y. acknowledges support from the University of Missouri-Columbia start-up fund. P.-Y.C. acknowledges support from the NSF Grant ECCS 1914420: CAREER. G.H. acknowledges support from the Air Force Office of Scientific Research under Grant AF 9550-18-1-0342 with Program Manager Dr. Byung-Lip (Les) Lee. S.D. acknowledges support from NIH under Grants R01NS069726 and R01NS094539.

1. T. R. Ray *et al*., Bio-integrated wearable systems: A comprehensive review. *Chem. Rev.* **119**, 5461–5533 (2019).
2. N. Matsuhisa, X. Chen, Z. Bao, T. Someya, Materials and structural designs of stretchable conductors. *Chem. Soc. Rev.* **48**, 2946–2966 (2019).
3. M. Bariya, H. Y. Y. Nyein, A. Javey, Wearable sweat sensors. *Nat. Electron.* **1**, 160–171 (2018).
4. S. Yang *et al*., "Cut-and-paste" manufacture of multiparametric epidermal sensor systems. *Adv. Mater.* **27**, 6423–6430 (2015).
5. K. Sim, Z. Rao, F. Ershad, C. Yu, Rubbery electronics fully made of stretchable elastomeric electronic materials. *Adv. Mater.* **32**, 1902417 (2020).
6. J. Kim, A. S. Campbell, B. E. F. de Ávila, J. Wang, Wearable biosensors for healthcare monitoring. *Nat. Biotechnol.* **37**, 389–406 (2019).
7. W. Gao, H. Ota, D. Kiriya, K. Takei, A. Javey, Flexible electronics toward wearable sensing. *Acc. Chem. Res.* **52**, 523–533 (2019).
8. D. C. Kim, H. J. Shim, W. Lee, J. H. Koo, D. H. Kim, Material-based approaches for the fabrication of stretchable electronics. *Adv. Mater.* **32**, 1902743 (2020).
9. T. Someya, M. Amagai, Toward a new generation of smart skins. *Nat. Biotechnol.* **37**, 382–388 (2019).
10. T. Someya, Z. Bao, G. G. Malliaras, The rise of plastic bioelectronics. *Nature* **540**, 379–385 (2016).
11. F. Molina-Lopez *et al*., Inkjet-printed stretchable and low voltage synaptic transistor array. *Nat. Commun.* **10**, 2676 (2019).
12. N. Matsuhisa *et al*., Printable elastic conductors by in situ formation of silver nanoparticles from silver flakes. *Nat. Mater.* **16**, 834–840 (2017).
13. Z. Zou *et al*., Rehealable, fully recyclable, and malleable electronic skin enabled by dynamic covalent thermoset nanocomposite. *Sci. Adv.* **4**, eaaq0508 (2018).
14. S. K. Kang, J. Koo, Y. K. Lee, J. A. Rogers, Advanced materials and devices for bioresorbable electronics. *Acc. Chem. Res.* **51**, 988–998 (2018).
15. D. Tobjörk, R. Österbacka, Paper electronics. *Adv. Mater.* **23**, 1935–1961 (2011).
16. G. Zheng, L. Hu, H. Wu, X. Xie, Y. Cui, Paper supercapacitors by a solvent-free drawing method. *Energy Environ. Sci.* **4**, 3368–3373 (2011).

17. X. Liao *et al*., Flexible and highly sensitive strain sensors fabricated by pencil drawn for wearable monitor. *Adv. Funct. Mater.* **25**, 2395–2401 (2015).
18. L. Malard, M. Pimenta, G. Dresselhaus, M. Dresselhaus, Raman spectroscopy in graphene. *Phys. Rep.* **473**, 51–87 (2009).
19. Z. Zhang, M. F. Iskander, J.-C. Langer, J. Mathews, Dual-band WLAN dipole antenna using an internal matching circuit. *IEEE Trans. Antenn. Propag.* **53**, 1813–1818 (2005).
20. N. J. Kirsch *et al*., "Optically transparent conductive polymer RFID meandering dipole antenna" in *2009 IEEE International Conference RFID*, (IEEE, Orlando, FL, 2009), pp. 278–282.
21. G. A. Casula, G. Montisci, G. Mazzarella, A wideband PET inkjet-printed antenna for UHF RFID. *IEEE Trans. Antenn. Propag.* **12**, 1400–1403 (2013).
22. A. Sarycheva *et al*., 2D titanium carbide (MXene) for wireless communication. *Sci. Adv.* **4**, eaau0920 (2018).
23. T. C. Shyu *et al*., A kirigami approach to engineering elasticity in nanocomposites through patterned defects. *Nat. Mater.* **14**, 785–789 (2015).
24. H. U. Chung *et al*., Binodal, wireless epidermal electronic systems with in-sensor analytics for neonatal intensive care. *Science* **363**, eaau0780 (2019).
25. Y. Xu *et al*., Multiscale porous elastomer substrates for multifunctional on-skin electronics with passive-cooling capabilities. *Proc. Natl. Acad. Sci. U.S.A.* **117**, 205–213 (2020).
26. B. Sun *et al*., Gas-permeable, multifunctional on-skin electronics based on laser-induced porous graphene and sugar-templated elastomer sponges. *Adv. Mater.* **30**, e1804327 (2018).
27. A. Miyamoto *et al*., Inflammation-free, gas-permeable, lightweight, stretchable on-skin electronics with nanomeshes. *Nat. Nanotechnol.* **12**, 907–913 (2017).
28. S. Chao *et al*., Synthesis and characterization of tigecycline-loaded sericin/poly (vinyl alcohol) composite fibers via electrospinning as antibacterial wound dressings. *J. Drug Deliv. Sci. Technol.* **44**, 440–447 (2018).
29. D. H. Kim *et al*., Epidermal electronics. *Science* **333**, 838–843 (2011).
30. Y. Ling *et al*., Laser-induced graphene for electrothermally controlled, mechanically guided, 3D assembly and human-soft actuators interaction. *Adv. Mater.* **32**, e1908475 (2020).
31. J. Kim, J. Hong, N. Kim, E. Cha, T.-S. Lee, "Two algorithms for detecting respiratory rate from ECG signal" in *World Congress on Medical Physics and Biomedical Engineering 2006*, R. Magjarevic, J. H. Nagel, Eds. (Springer, Berlin, Heidelberg, 2007), pp. 4069–4071.
32. F. Rosenow, K. M. Klein, H. M. Hamer, Non-invasive EEG evaluation in epilepsy diagnosis. *Expert Rev. Neurother.* **15**, 425–444 (2015).
33. K. G. Jordan, Emergency EEG and continuous EEG monitoring in acute ischemic stroke. *J. Clin. Neurophysiol.* **21**, 341–352 (2004).
34. G. Borghini, L. Astolfi, G. Vecchiato, D. Mattia, F. Babiloni, Measuring neurophysiological signals in aircraft pilots and car drivers for the assessment of mental workload, fatigue and drowsiness. *Neurosci. Biobehav. Rev.* **44**, 58–75 (2014).
35. N. H. Liu, C. Y. Chiang, H. C. Chu, Recognizing the degree of human attention using EEG signals from mobile sensors. *Sensors (Basel)* **13**, 10273–10286 (2013).
36. D. H. Ho *et al*., Multifunctional smart textronics with blow-spun nonwoven fabrics. *Adv. Funct. Mater.* **29**, 1900025 (2019).
37. S. Imani *et al*., A wearable chemical-electrophysiological hybrid biosensing system for real-time health and fitness monitoring. *Nat. Commun.* **7**, 11650 (2016).
38. Y. Yang *et al*., A laser-engraved wearable sensor for sensitive detection of uric acid and tyrosine in sweat. *Nat. Biotechnol.* **38**, 217–224 (2020).
39. W. He *et al*., Integrated textile sensor patch for real-time and multiplex sweat analysis. *Sci. Adv.* **5**, eaax0649 (2019).
40. C. Yang, Y. Huang, H. Cheng, L. Jiang, L. Qu, Rollable, stretchable, and reconfigurable graphene hygroelectric generators. *Adv. Mater.* **31**, e1805705 (2019).
41. T. Xu *et al*., An efficient polymer moist-electric generator. *Energy Environ. Sci.* **12**, 972–978 (2019).